Electrocatalysis of the nitrite reduction : a mechanistic study

Duca, M.

2

New insights into the mechanism of nitrite reduction on a platinum electrode

Abstract

This chapter reinvestigates the mechanism of HNO_2 and NO_2^- reduction on polycrystalline platinum as a function of electrolyte pH and reactant concentration. Intermediates and/or reaction products were detected by means of various (combined) techniques: RRDE (for NH_2OH detection), OLEMS (for volatile products) and FTIRS. In acidic media, HNO_2 is depleted due to homogeneous-phase reactions (accelerated by stirring) that generate NO: the latter species, which readily forms an adlayer on Pt, is reduced in a first wave to N_2O, while HNO_2 is reduced in a following diffusion-limited wave to mainly NH_2OH. The two waves display different reaction orders. Loss of HNO_2 (as NO) in the blanketing Ar stream hampered an accurate quantitative evaluation of the product distribution. When the pH is increased, NO_2^- is reduced in a single peak with a much lower current density than in the previous case. In RDE experiments, the peak was found to decrease with increasing rotation rates. The presence of a sluggishly reduced intermediate (NH_2OH) has been proposed. A general mechanistic scheme, including NO, HNO_2 and NO_2^-, is discussed.

This chapter has been published in: Duca, M.; Kavvadia, V.; Rodriguez, P.; Lai, S. C. S.; Hoogenboom, T.; Koper, M. T. M. *J. Electroanal. Chem.* **2010**, *649*, 59-68.

2.1. Introduction

The reduction of nitrite/nitrous acid has attracted widespread attention from both applied and fundamental points of view[1-7]. Being a pollutant of groundwater, nitrite is the target of various removal processes, and electrochemical reduction could become competitive provided that selectivity to a non-polluting (N_2) or useful (NH_2OH) material is achieved.

From a fundamental point of view, the electrochemical behavior of nitrite/nitrous acid plays a central role in the complex reaction pathways that compose the electrochemical nitrogen cycle[7]. For instance, when in contact with transition-metal electrodes such as platinum or rhodium, NO adlayers are readily formed from acidic solutions of nitrite[4,8]. Furthermore, in nitrate reduction on coinage and noble metals in acidic media, the first step, i.e. $NO_3^- \rightarrow NO_2^-$, has been considered as the rate determining step by various groups[9,10], and the selectivity of the overall reaction sensitively depends on the subsequent reduction of nitrite and NO_{ads}. Finally, nitrite is active in various solution phase reactions, especially at low pH[11-14], although the precise influence of these reactions on the electrochemical reactivity is poorly understood.

Previous research on nitrite reduction on platinum in acidic media with rotating-ring disk electrodes (RRDE)[1], differential electrochemical mass spectroscopy (DEMS)[1,15] and Fourier-Transform Infrared Spectroscopy (FTIRS)[6], has highlighted two major mechanistic pathways taking place in acidic solutions in the millimolar nitrite concentration range: diffusion-controlled formation of NH_2OH, at potentials close to hydrogen evolution (ca. 0.1 V vs. RHE), and formation of N_2O, detected by DEMS and FTIRS, at higher potentials (0.3-0.5 V vs. RHE).

Gadde and Bruckenstein[1] detected hydroxylamine with RRDE voltammetry and, under the assumption that hydroxylamine and nitrous acid do not react with each other, it was concluded that the current yield of this product is ca. 60 %. This observation, paired with the reported number of electrons from RRDE voltammetry, $n = 3.83$ ($n = 4$ corresponds to NH_2OH), led Gadde and Bruckenstein to speculate about the possible disproportionation of NH_2OH to NH_3 and N_2O as the cause of the less than 100% yield in NH_2OH. Using DEMS, the same authors observed the formation of N_2O, which was confirmed in a later study by Scherson et al.[6] by means of FTIRS.

In order to reach a more accurate description of the mechanism, the relevance of the nitrous acid decomposition (in the acidic pH range) needs to be addressed. The value of pK_a for HNO_2 is reported between 3.16[16] and 3.37[17]; therefore, HNO_2 will clearly be the dominant species for pH < pK_a, along with hydrated nitrosonium ions ($H_2NO_2^+$)[14]. The decomposition behavior of nitrous acid can be described by the following equilibria[12]:

$$2HNO_2 \rightleftharpoons NO + NO_2 + H_2O \quad (1)$$

$$2NO_2 \rightleftharpoons N_2O_4 \quad (2)$$

$$N_2O_4 + H_2O \rightleftharpoons HNO_2 + HNO_3 \quad (3)$$

In previous reports[18,19] it was suggested that HNO_2 decomposition strongly depends both on the forced convection of the system (such as rotation rate of the disk or stirring) and on the flow of gas blanketing the surface, as both of these variables influence the rate of the removal of the NO produced from the system by reaction (1). As early as 1922, Klemenc and Pollak[20] recognized NO removal as the rate determining step. Further evidence on the importance of NO removal was published more recently by Beake et al.[13], who studied nitrous acid decomposition in oxygen-purged acidic nitrite solutions. Nitrous acid decomposition has indeed been cited in previous electrochemical studies[1,6,7] devoted to nitrite reduction, but without considering this reaction as a major actor in the mechanism of HNO_2 reduction. Yet, decomposition will always take place in the entire pH range where nitrous acid is present; for a dilute solution, a reasonable upper limit is within three units of the pK_a value. The electrochemistry of the nitrite ion, without any interference from other species, can therefore only be probed in alkaline media.

Reactions (1) - (3) suggest that formation of NO is not only restricted to the surface of the transition metals, as referred to above, but is also formed in the solution, generating a species[12] that reacts electrochemically on Pt in the same potential region as the reduction of nitrous acid itself[21].

The present chapter has two main objectives: to obtain further evidence that the electrochemical reduction of nitrous acid is accompanied and influenced by homogeneous chemical reactions, and, consequently, to detect the actual products of nitrous acid reduction (in particular NH_2OH and N_2O) by means of traditional

electrochemical techniques combined with spectroscopy (FTIRS, OLEMS), in order to draw a more comprehensive mechanistic picture.

2.2. Experimental

All glassware was cleaned following a standard procedure[22] to remove all traces of organic contaminations. Electrolyte solutions were prepared with Suprapur (Merck) reagents and Millipore MilliQ water (resistivity >18.2 MΩ cm); prior to the experiments oxygen was removed by bubbling argon (purity grade 6.0) through the solution for at least 15 minutes. Argon blanketing was used to protect the solutions during the experiments. $NaNO_2$ (Merck, p.a., ACS grade) was used after drying at 70 °C overnight and then stored in a desiccators under vacuum. Concentrations reported in this chapter are nominal and, when nitrous acid decomposition takes place, are to be considered as starting (upper-limit) concentrations. Phosphate buffer solutions (ionic strength 0.1 M) were prepared for experiments at $2 < pH < 4$; the pH was checked before and after the experiments with a Radiometer Copenhagen pH meter. No noticeable pH change was observed during the experiments.

An Autolab PGSTAT20 (bi-)potentiostat was used throughout this work. Transfer and stationary experiments were carried out with a Pt flag electrode (geometrical area 2.30 cm^2); prior to use, it was flame-annealed and quenched in water saturated with an $Ar:H_2$ 3:1 atmosphere[23]. For all electrochemical experiments the counter electrode was a platinum flag or wire, which was also flame-annealed and quenched in air. A Reversible Hydrogen Electrode (RHE) was employed as reference electrode for all experiments, and all potentials reported in this chapter are relative to the RHE.

Rotating disk platinum electrodes (diameter 5 mm) were used in a Pine Instrument Ring-Disk Teflon tip equipped with a Pt ring; rotating disk (RDE) and rotating ring-disk (RRDE) experiments were performed with a Pine Instrument motor generator (MSR rotator). The experimental collection efficiency was 0.26 ± 0.03 as calculated with the reversible couple $[Fe(CN)_6]^{-4}/[Fe(CN)_6]^{-3}$. A different cleaning procedure was used for the RRDE tip: after assembling the disk insert, the tip was immersed in a slightly acidic concentrated $KMnO_4$ solution for several hours. Next, the tip was treated with an H_2O_2-H_2SO_4 solution and thoroughly rinsed with MilliQ water to remove all traces of the cleaning procedure. The whole tip was then

polished using a Buehler polishing cloth and 0.05 μm Al_2O_3. As a final cleaning step, both the ring and the disk electrodes were cycled between the oxygen and hydrogen evolution potentials in an auxiliary cell containing the working electrolyte, until a stable voltammogram was obtained. Finally the tip was rinsed with MilliQ water and transferred to the working cell immediately before the experiment.

Adsorbate studies were performed using the following transfer procedure[21]: the flag electrode was immersed in a nitrite-containing solution (0.8 mM) of a chosen electrolyte under potential control (0.6 V vs. RHE) for 120 seconds, rinsed and then protected with a droplet of water during the transfer to another cell containing clean electrolyte. The nitrite concentration chosen for the adsorption step equals the one used in stationary continuous reduction experiments (0.8mM).

FTIRS experiments were carried out under external reflection configuration using a Brucker Vertex 80v spectrometer. The cell for spectroelectrochemical experiments was equipped with a CaF_2 prism beveled at 60º. At each potential, 50 interferograms at 6 cm^{-1} were collected. The reflectance spectra reported throughout the chapter are plotted as $(R–R_0)/(R_0)$, where R and R_0 are the reflectance at the sample and at the reference potential, respectively. Hence, in such plots the appearance of bands pointing up is typical of species consumed at the sample potential with respect to the reference potential, while bands pointing down indicate the appearance of a species. The potential was changed following a staircase profile: details will be given later. The same setup was also used for Attenuated Total Reflection (ATR) experiments carried out to investigate the solution species: in this case 100 interferograms were collected at 8 cm^{-1}.

On-Line Electrochemical Mass Spectrometry (OLEMS) [24] measurements were performed on an EvoLution mass spectrometer system (European Spectrometry Systems Ltd). The system consists of a Prisma QMS200 (Pfeiffer), brought to vacuum with a TMH-071P turbo molecular pump (60 l s^{-1}, Pfeiffer) and a Duo 2.5 rotary vane pump (2.5 m^3 h^{-1}, Pfeiffer). During measurements, the pressure inside the MS was $1 - 5 \cdot 10^{-6}$ mbar.

The reaction products at the electrode interface were collected through a small inlet tip positioned close (~ 10 μm) to the electrode surface by means of a micrometer system and a camera[24]. The inlet tip is constructed from a Kel-F holder, with an

inner diameter of 0.52 mm, into which a small porous Teflon cylinder (Porex) of 0.60 mm diameter with an average pore size of 5 μm is squeezed. The inlet was connected to the MS through a PEEK capillary with an inner diameter of 1/16 inch (1.59 mm). The tip configurations was cleaned in a solution of 0.2 M $K_2Cr_2O_7$ in 2 M H_2SO_4 and rinsed thoroughly with ultra-pure water before use.

2.3. Results

2.3.1 Nitrite reduction and adsorbate stripping on Pt stationary electrodes.

Nitrite reduction was investigated under stationary conditions in three different electrolytes, 0.5 M H_2SO_4, 0.1 M $HClO_4$ and a phosphate buffer at pH 3. The voltammetric profile for nitrite reduction at a stationary Pt electrode in 0.1 M $HClO_4$ is reported in Figure 1, along with the profile for the adsorbate stripping in the same electrolyte (negative-going scans only). In the latter case a single sweep up to 0.05 V is sufficient to recover the blank Pt profile in the first positive-going scan (not shown), as has already been reported for NO adlayers generated from NO-saturated solutions[21] and from acidic nitrite solutions[8,21]. Two main features can be recognized for the continuous reduction: a reduction "first wave" between 0.5 and 0.3 V, and a broad second wave, possibly composed of two sub-peaks, between 0.3 and 0.1 V. This first wave has never been reported in this concentration range, although Scherson et al. obtained a current in the same potential region for a stationary Pt electrode at higher nitrite concentrations (20 mM)[6].

Comparing the adsorbate stripping profile with the continuous reduction, the high-potential first wave is absent for the adsorbate; adsorbate reduction starts at ca. 0.35 V with a succession of peaks in the same potential region as the broad main peak potential of the continuous nitrite reduction. The current density, however, is much lower for the adsorbate stripping. The charge involved in the reductive stripping, corrected for hydrogen adsorption, is 326 μC cm^{-2}, comparable with previous results[21]. (The lower charge – i.e. the lower coverage – reported with respect to the paper cited is consistent with the lower nitrite concentration used in our experiment).

Voltammetric profiles similar to those shown in Figure 1 were measured for all three electrolytes under investigation with only minor differences. The most

remarkable feature of the stripping experiment of the adlayer generated in phosphate buffer (pH 3) is the lower charge involved in the stripping process, with a corrected value of 156 μC cm^{-2}, indicating a lower value of the corresponding NO coverage.

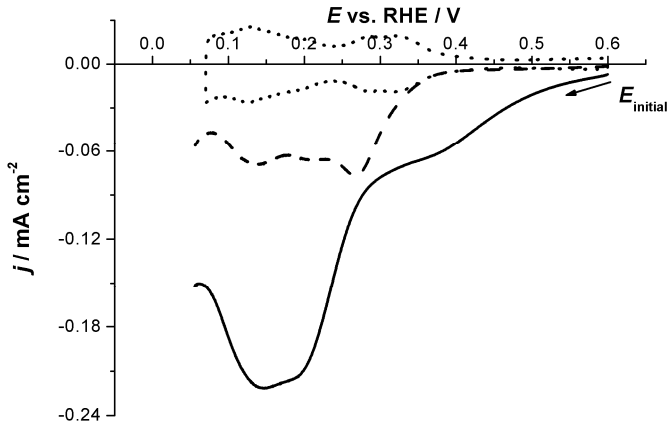

Figure 1 Voltammetric profiles for continuous nitrite reduction (first cycle, bold line) and for adsorbate stripping (dashed line) on a polycrystalline Pt electrode in 0.1 M $HClO_4$ (blank CV, dotted line). Nitrite concentration (for continuous reduction and for adsorbate generation) 0.8 mM. Starting potential 0.6 V. v = 20 mV s^{-1}.

2.3.2 Nitrite reduction at RRDE.

In order to avoid the uncertainties due to the diffusion limitations mentioned in the introduction, nitrite reduction was examined at a rotating ring-disk electrode assembly [25] with a Pt ring and a Pt disk. The ring-disk experiments were carried out to obtain additional information on the product distribution and the reaction mechanism.

2.3.2.1 Dependence of the voltammetric feature on the nitrite concentration and the pH

The influence of the nitrite concentration was investigated in a series of cyclic voltammetry scans in a phosphate buffer (pH 3). This medium was chosen because the nitrous acid decomposition becomes slower as the pH is raised, thus allowing for a longer working time and better control of the concentration.

With the exception of the work of Gadde and Bruckenstein[1], most previous research has dealt with fairly concentrated (supramillimolar)[6,8,26,27] nitrite solutions; nevertheless, Figure 2 shows that the overall features of nitrite reduction can be better appreciated and compared with one another by extending the concentration range to lower values.

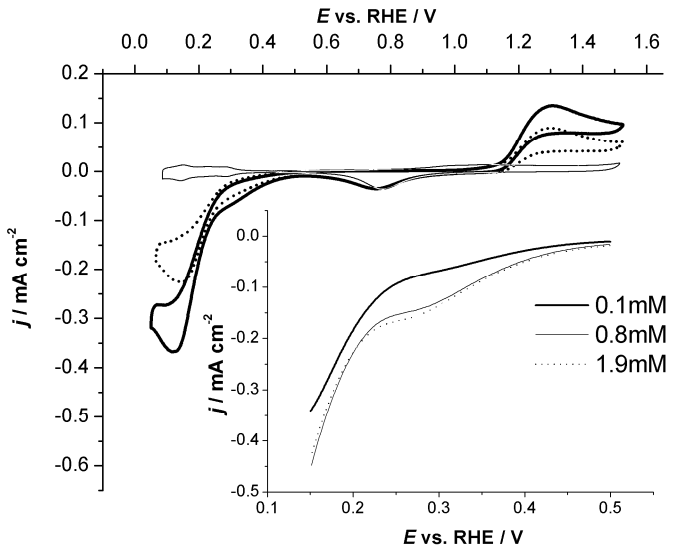

Figure 2 Influence of nitrite concentration (50 μM-1.9 mM) on the reduction profile of nitrite/nitrous acid in a 0.1 M phosphate buffer (pH 3) at a rotating Pt electrode. Main figure: dotted line 50 μM, bold line 0.1 mM, thin line blank voltammetry. Inset: highlight on the first wave. ω = 900 rpm, v =10 mV s^{-1}.

The cyclic voltammograms reported in Figure 2 include low-concentration (0.05 and 0.1 mM) and high-concentration experiments (up to 1.9 mM). The former are consistent with those reported by Gadde and Bruckenstein[1] for similar concentrations in 0.1 M $HClO_4$: the limiting reduction current is better defined during the positive-going scan whereas a peaked feature appears in the negative-going sweep. Upon increase of the concentration above 0.1 mM (see figure 2 and inset), the high-potential reduction first wave clearly appears as a separate signal in the potential region between 0.2 and 0.45 V. The first wave and the second wave respond differently to the concentration: the former displays a reaction order lower than 0.3, eventually becoming saturated above 1.9 mM, while the latter shows a reaction order close to 1.

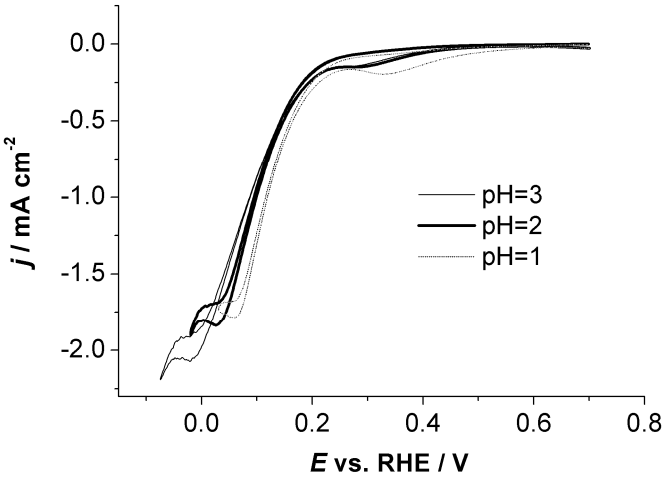

Figure 3 Comparison between the voltammetric profiles of nitrite (0.8 mM) in a 0.1 M phosphate buffer (pH = 3, thin full line), in 0.01 M $HClO_4$ + 0.09 M $KClO_4$ (bold line) and 0.1 M $HClO_4$ (small dotted line) at a Pt rotating disk electrode, ω = 900 rpm, v =10 mV s^{-1}.

In analogy to the experiments reported in Section 2.3.1, a concentration of 0.8 mM was chosen to investigate the effect of pH on the reduction wave. Typical reduction profiles for this concentration are shown in Figure 3. With increasing pH, the plateau-like region progressively shifts to more negative potentials on the RHE scale, entering the region of hydrogen evolution for a pH value equal to 3. The plateau-like current tends to increase with pH, although it must be pointed out that, as it will be shown in the following section, a direct comparison between the limiting currents recorded in different experiments is not straightforward due to the decomposition of nitrous acid. More interestingly, the voltammogram at more positive potentials (> 0.2 V) is dominated by a first-wave signal which never reaches a real plateau current and is present only during the negative-going scan. This first wave noticeably broadens and reaches a higher j in more acidic media (Figure 4), while it is almost invisible at pH 3.5 (the highest pH analyzed).

2.3.2.2 Evidence for decomposition of nitrous acid.

Qualitative evidence for nitrous acid decomposition may be obtained in a potentiostatic experiment in which the potential is kept constant at a value in the plateau-like region of the reduction curve and the limiting current is measured with time; at a constant rotation rate, the current should be proportional to the

concentration according to Levich equation[28]. This method has already been used previously[26,27,29] to correct for the progressive depletion of nitrous acid. However, being aware of the uncertainties inherent in such an approach (primarily related to the role of solution stirring) , we do not aim to use this method to correct our data.

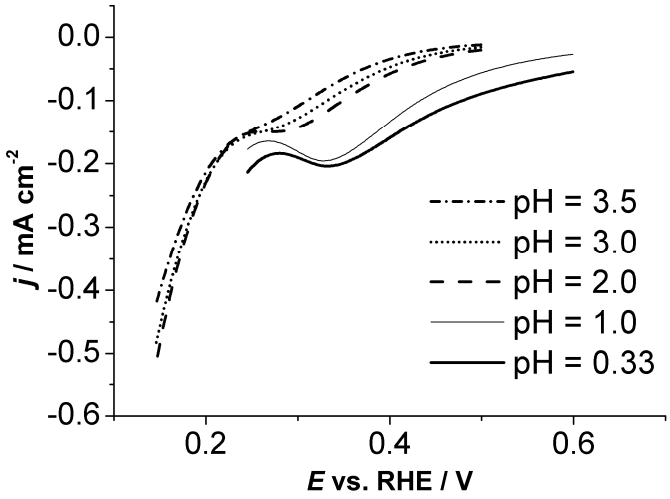

Figure 4 High-potential first wave detected during the reduction of nitrite (0.8 mM) in various electrolytes at a Pt rotating disk electrode, ω = 900 rpm, v = 10 mV s^{-1}.

After recording the I / t curve, a standard kinetics analysis can be applied to obtain the *apparent* reaction order by fitting the data to one of the characteristic equations featuring the concentration as a function of time; in our case, the best fit is obtained for $1/I$ as a function of t, equivalent to apparent second-order kinetics [30]. Figure 5 displays this trend in time for the normalized limiting current ($I_{lim}(t)/I_{lim,}$ (t = 0)) for a 0.8 mM nitrite solution in 0.1 M $HClO_4$ and 0.1 M phosphate buffer (pH=3). To our knowledge, this observation has never been reported before for an electrochemical experiment, although a second-order decomposition at pH 3.1 was mentioned in the paper by Park et al. [12] and in unpublished results cited in Younathan et al.[31]. The complex dependence of nitrous acid decomposition on the flow rate of blanketing gas does not allow quantitative comparison between different experiments conducted in an electrochemical cell where accurate control over the gas flow may not be attained. Nevertheless, Figure 5 shows that a decrease

in pH has a noticeable effect on the decomposition rate, for the same starting concentration, suggesting a faster decomposition at lower pH.

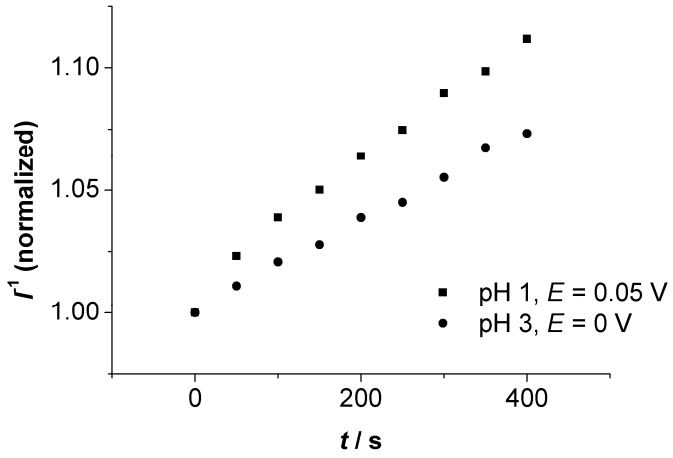

Figure 5 Plot of I^{-1} (normalized) *vs.* time for the decomposition of 0.8 mM nitrite in 0.1 $HClO_4$ and in 0.1 M phosphate buffer (pH 3), ω = 900 rpm, E = 0.05 V and E = 0 V, respectively

In order to support our observations and to exclude that the decrease in limiting current is due to the time-dependent adsorption of a poisoning species, we compared the limiting currents in subsequent cycles of CV scans. Since the half-life for a second-order reaction is $kC_{\text{reactant}}^{-1}$, we chose to carry out this test at a lower nitrite concentration (50 μM) to study a slower decomposition process (although the decomposition cannot be suppressed even at such low concentrations, as shown by Park et al.[12]). In addition, a slower decomposition rate will ensure that less NO has been produced, thus reducing the influence of this species. Table 1 illustrates the qualitative trends in the decrease of plateau-like currents in successive cycles as a function of pH and with rotation rate (equivalent to stirring of the solution, which is also known to accelerate the decomposition of nitrous acid, as mentioned above). In agreement with previous work[19], maximum decomposition rates have been obtained for more acidic solutions and at higher rotation rates. As a comparison between Table 1 and Figure 5, the depletion of nitrous acid over 300 s is equal to ca. 8% when C_{nitrite} = 0.8 mM and 4% when C_{nitrite} = 50 μM (at pH 1).

Time-dependent ATR infrared experiments were carried out in 0.8 mM $NaNO_2$ solution of various pH values to highlight the more significant formation of NO at lower pH. Unfortunately, it was not possible to ascertain the change in the quantity of NO formed. Nonetheless, the time evolution of the spectra at pH 1 and at pH 3 show the appearance of a weak band at 2330 cm^{-1}, especially at pH=1, that could be assigned to the N-O stretching frequency of H_2ONO^+ on the basis of previous experimental[14] and computational[32] studies.

pH	Decrease in I_{lim}, two successive cycles, 50 µM, 900 rpm.	Decrease in I_{lim}, two successive cycles, 50 µM, 2900 rpm.
4.0	0.1 %	0.8 %
3.5	0.9 %	1.5 %
3.0	3.0 %	4.0 %
1.0	4.0 %	6.0 %
0.33	5.5 %	8.4 %

Table 1 Decrease in limiting current during voltammetry in various electrolytes, $NaNO_2$ concentration 50 µM, at two different rotation rates.

2.3.2.3. The first-wave signal: N_2O formation.

More insight into the nature of the first wave was obtained by using a Pt rotating disk electrode in 0.1 M $HClO_4$. The first wave can be observed clearly at scan rates lower than or equal to 50 mV s^{-1}, and a rotation rate of 900 rpm; therefore, a scan rate of 10 mV s^{-1} was chosen for all experiments. When the potential window is restricted to 0.04 – 0.6 V, a decrease in the first-wave profile takes place in the second cycle. The original profile of the first wave can only be recovered by keeping the electrode at 0.6 V for 1 min before scanning the potential again in the negative direction. As diffusion limitations can be ruled out, the observed phenomena could be attributed to the slow adsorption (on the timescale of the voltammetric sweep) of a species, which takes place at ca. 0.6 V. During the scan, the initial coverage of this species at 0.6 V cannot be recovered unless the potential

is held constant at this value for sufficient time; consequently, the lower surface availability of the reacting species causes a lower current of the first wave.

RRDE experiments are shown in Figure 6. The nitrous acid reduction current is measured at the ring (I_{ring}) at constant E_{ring} = 0.08 V during potential sweep at the disk in 0.01 M $HClO_4$ + 0.09 M $KClO_4$ (pH 2). The ring current is therefore a measure of the nitrous acid consumption at the disk. Figure 6a was recorded with a 0.8 mM $NaNO_2$ concentration. During the negative-going scan, I_{ring} decreases in the same potential range where the high potential first wave is detected at the disk (0.6 – 0.3 V), whereas during the positive-going sweep in the same potential range I_{ring} remains constant. The profile of the decreasing ring current in the high-potential region, in addition, is also not as steep as at more negative potentials, suggesting two different processes. As shown in Figure 2, experiments carried out in the micromolar range display a less pronounced first wave. To obtain additional data about the concentration dependence of the high-potential reduction process, we repeated the RRDE experiment for a 50 μM $NaNO_2$ solution at pH 2. Figure 6b shows that I_{ring} decreases monotonically during the negative-going scan until the disk potential reaches the plateau-like region of nitrite reduction, subsequently retracing almost the same line during the positive-going scan, with only minor differences in the 0.4 – 0.5 V potential range. Therefore, high-concentration RRDE experiments add more details to the scenario sketched in the previous paragraph for the process underlying the high-potential first-wave: nitrous acid consumption is enhanced and/or induced during the potential excursion 0.6 → 0.3 V by the presence of an (adsorbed) species which is absent in the subsequent scan 0.3 → 0.6 V.

In order to obtain additional information on the intermediates and on the product distribution in the potential region corresponding to the first wave, we employed in situ FTIRS. The experiments were carried out on a polycrystalline Pt electrode in a phosphate buffer (0.1 M, pH = 3) in the presence of 0.8 mM $NaNO_2$. The spectra were collected in the potential range 0.65 – 0.2 V and the reference potential (corresponding to the R_0 values) was 0.65 V. The potential was stepped to more negative values by 50 mV steps; between each step, the electrode was kept at 0.6 V for 2 min, in order to avoid the previously mentioned “hysteresis effect” of the first wave.

Figure 7 shows a selected region of the IR spectrum, at different potentials. The dominant feature of the spectra is a peak centered at 2231 cm^{-1}, which starts to appear at 0.5 V, the potential corresponding to the onset of the first wave during a RDE experiment at the same pH (see Figure 8). This peak can be confidently assigned to the asymmetric stretch (v_1) of N_2O, on the basis of the known infrared spectrum of N_2O[33]. Figure 7b displays the integrated band intensities of the signal at 2231 cm^{-1}, an indicative measure of the consumption / formation of the species observed in the thin layer; the trend shows that the removal of N_2O from the thin layer starts between 0.35 V and 0.3 V.

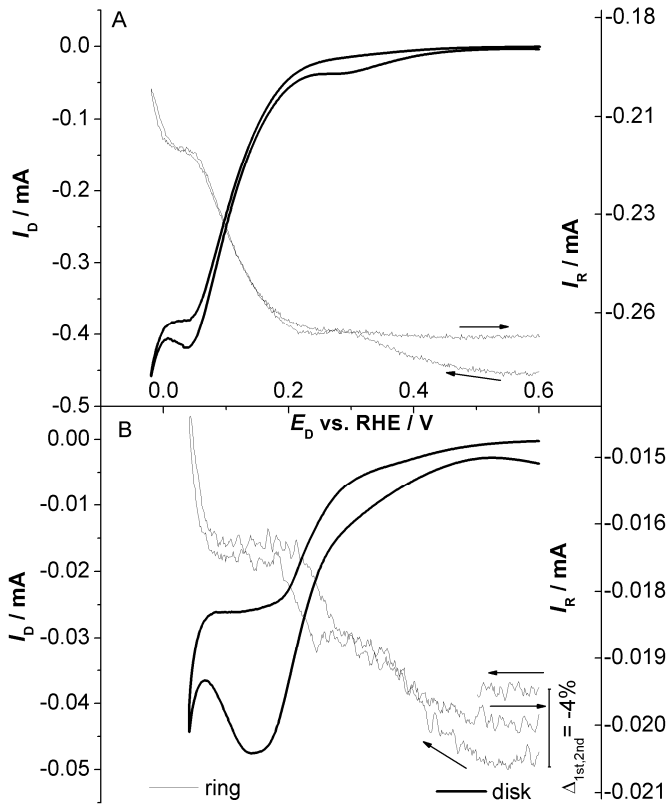

Figure 6 Comparison between the current recorded at a Pt disk (I_D) during potential scan (ω = 1200 rpm, v = 10 mV s^{-1}) and at a Pt ring (I_R , E_{ring} = 0.08 V) during reduction of 0.8 mM (A) nitrite and 50 μM (B) in 0.01 M $HClO_4$ + 0.09 M $KClO_4$, pH 2.

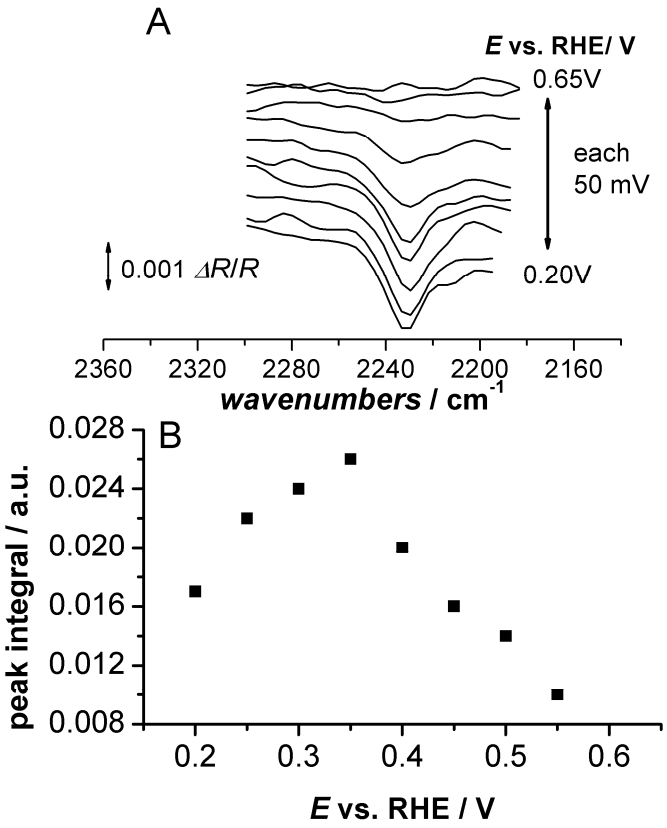

Figure 7 A) Potential difference FTIR spectra collected at a polycrystalline Pt electrode in a phosphate buffer (0.1 M, pH 3) containing 0.8 mM $NaNO_2$. Reference potential 0.65 V, *p*-polarized light. B) Trends of the integrated area of the peak at 2231 cm^{-1} vs. potential; for the integration a linear baseline was used.

OLEMS experiments also provided further confirmation of the formation of N_2O. The formation of volatile products was measured during reduction in 0.1 M H_2SO_4, with a nitrite concentration slightly higher than usual (1.4 mM). The plot of the ion current as a function of potential is shown in Figure 8: the ion current for *m/z* 44 (N_2O) increases while scanning the potential in the negative direction and reaches a maximum between E = 0.35 and 0.4 V. The ion current reached in the backward (positive-going) scan is lower and this difference can be compared to the previously mentioned similar observations made with the RRDE. The second signal shown, *m*/*z* 30, corresponds to NO and is the combination of two contributions: the stream of NO and the fragmentation of N_2O in the mass

spectrometer. The *m*/*z* 30 signal decreases with decreasing potential, reaching a constant value in the low-potential region (corresponding to the second wave of the voltammogram, see Section 2.3.2.4.). This shows that NO from the solution is consumed during the formation of N_2O, and this consumption overcomes the fragmentation of the N_2O in the MS setup, whose contribution can be still recognized in the potential region $0.25 < E < 0.4$ V of the MS trace.

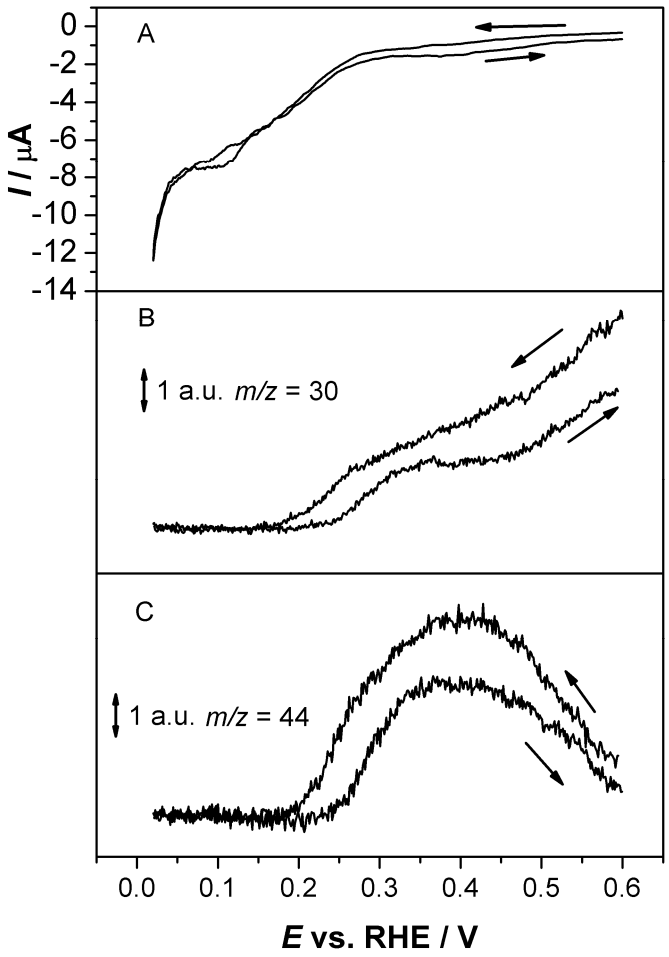

Figure 8 Cyclic voltammetry during OLEMS measurements (A) and ion current intensity profiles for *m*/*z* = 30 (B) and 44 (C) in 0.1 M H_2SO_4 containing 1.4 mM $NaNO_2$. Working electrode was a polycrystalline Pt electrode, $v = 1$ mV s^{-1}. The arrows indicate the direction of the potential sweep.

2.3.2.4. The second wave: Hydroxylamine (HAM) formation.

As already shown by Gadde and Bruckenstein[1], nitrite reduction in the low-potential region yields mainly hydroxylamine as a product. The most straightforward qualitative test to highlight the formation of NH_2OH (HAM) is a shielding ring-disk experiment, because HAM gives a peculiar "loop-shaped" oxidation signal during cyclic voltammetry[1], the current being higher during the negative-going scan than during the positive-going scan the range 1 – 1.2 V. An experimental proof that this is indeed a hydroxylamine fingerprint can be obtained by cycling voltammetry of equimolar solutions of nitrite and hydroxylamine[1]: the loop can be seen for $0.33 < pH < 3$. At higher pH values HAM is even more oxidizable and there is no longer a loop but the current for HAM oxidation is higher in the negative-going scan within a much wider potential window. Detailed analysis of this voltammetric feature was reported by Rosca et al.[34] where it was ascribed to enhanced HAM oxidation during the negative-going scan due to higher reactivity of the platinum surface following oxidative removal of NO_{ads} in the previous positive-going sweep.

Figure 9 shows the results of a typical RRDE experiment for 0.8 mM $NaNO_2$ in the most favorable pH range for hydroxylamine detection ($1 \leq pH \leq 2$); in the reduction region, there is a decrease in the plateau-like current when the disk is kept at 0.07 V compared to when the disk is kept at open circuit potential, whereas a minor increase in current is noticed in the oxidation region. More importantly, the loop-shaped signal is clearly detected in the oxidation branch, which suggests the presence of hydroxylamine. Following the arguments of Gadde and Bruckenstein[1], the ring current may be thought of as a sum of currents ascribable to the oxidation of HNO_2 and NH_3OH^+. It must be noted, however, that this is an approximation which is true only if the two molecules do not react with each other, a condition which is apparently not completely fulfilled[34-36] for the present case. While the oxidation current will be mainly influenced by the presence of a highly electroactive species such as hydroxylamine, the decrease in reduction current is mainly explained in terms of the shielding of the ring due to nitrous acid consumption at the disk. In our case, the ratio $I_{R,\ shielded}$ / $I_{R,\ unshielded}$ (shielded referring to E_{disk} = 0.07 V, unshielded to the situation where the disk is at open circuit potential, o.c.p.) is equal to 0.72, lower than the expected S value calculated from the electrode geometry and the experimental collection efficiency (0.77). It seems, therefore, that some nitrous acid is depleted during the transfer from the

disk to the ring, possibly due to its reaction with the hydroxylamine that is produced at the ring.

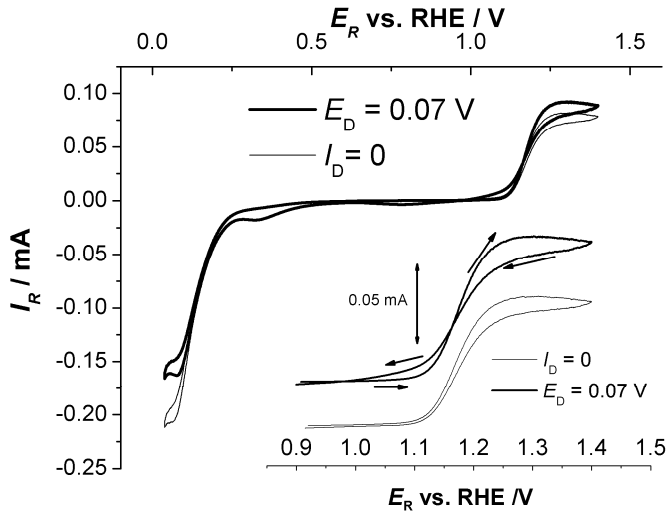

Figure 9 Profile of the ring current during a shielding experiment (ω = 900 rpm, v = 10 mV s^{-1}) in 0.1 M $HClO_4$ + 0.8 mM $NaNO_2$. Bold line depicts ring current with E_{disk} = 0.07 V and thin line with disk at open circuit potential. Inset: highlight of the crossover feature, with the bold line shifted to higher currents for better appreciation.

Interestingly, despite the increasingly noticeable oxidative behavior of HAM at higher pH, no loop was observed when the shielding experiment was carried out at pH 3; in this case, however, the disk potential was shifted to a more negative value to follow the corresponding shift of the plateau-like signal (see figure 3). On the other hand, the shielding at the ring can still be detected, and the ratio $I_{R,\ shielded}$ / $I_{R,\ unshielded}$ is equal to 0.77, on a par with the shielding constant of the system calculated from the experimental collection efficiency. Although it must be remembered that the collection efficiency for a non-purely diffusion-controlled process may be at variance with the value for diffusion-controlled reaction, this could be further evidence that in this case no hydroxylamine is formed, and that there is no reaction of nitrous acid with HAM in the disk-to-ring transfer.

Data analysis of diffusion-limited RDE experiments is usually carried out by plotting the values of the limiting current at different rotation rates according to the Levich equation. Given the presence of nitrous acid decomposition (see Section 2.3.2.2), which introduces uncertainties in the value of the nitrite concentration

used in this equation, it is extremely important to carry out the experiments immediately after nitrite has been added to the clean electrolyte. A typical Levich plot for I_{lim} of the reduction of 0.8 mM $NaNO_2$ in 0.1 M $HClO_4$ over the range 400-2900 rpm is shown in Figure 10. It displays once more the importance of the timescale: a plot having a lower slope is recorded 1 hour after the addition of the analyte, the solution being protected from air with Ar blanketing; the ratio of the slopes is 0.76. The quality of the fitting is fairly good (R^2 = 0.996) although the trend seems to deviate from a linear behavior at higher rotation rates; an additional piece of information is the non-zero intercept. In the high-concentration experiments, calculation of the number of electrons of the overall electrode process (n) from the Levich equation may be affected by several sources of error. Although the analysis is carried out in the shortest time possible, the "stirring effect" cited in the Introduction (increase of homogeneous-phase nitrous acid decomposition with increasing rotation rate) could influence the accuracy of n. Values of n = 3.1 are obtained for pH 1 and pH 2, whereas the value for pH 3 is n = 6.0 (E = 0 V), suggesting the formation of ammonia. Evidence of the formation of a more reduced product than NH_2OH is also shown in figure 3, where the limiting current density at pH 3 is higher than at pH 1 or 2.

The influence of the rotation rate on the limiting current was also investigated for the low-concentration case (50 μM $NaNO_2$). This concentration range was chosen in the hope of minimizing the influence of the homogeneous-phase decomposition. Linear Levich plots were measured, all of them having non-significant non-zero intercepts. The number of electrons calculated with Levich equation increases with increasing pH at constant potential (the shift mentioned in Figure 3 is not observed for 50 μM) and becomes equal to 4.0 for 3.5 ≤ pH ≤ 4. Reference tables or previous publications were used to retrieve the diffusion coefficients[27] and the kinematic viscosity[17].

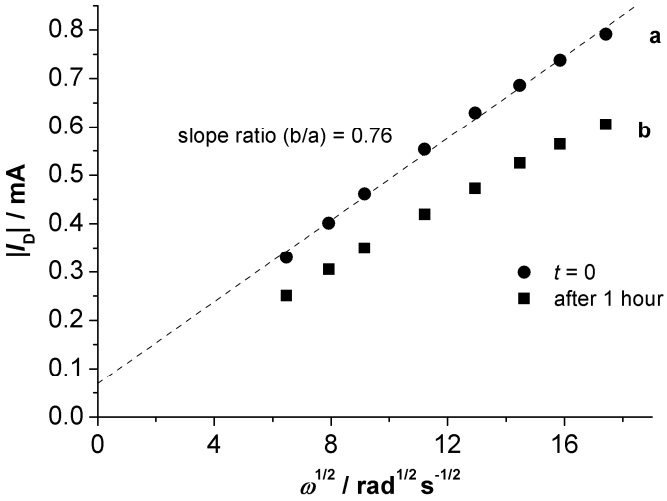

Figure 10 Levich plot for a 0.8 mM $NaNO_2$ solution in $HClO_4$, E = 0.07 V, as a function of the time elapsed from the addition of nitrite to the clean electrolyte.

2.3.2.5 Reduction in alkaline media

The reductive behavior of nitrite at alkaline pH (NaOH 0.1 M) is remarkably different, both qualitatively and quantitatively, as shown in Figure 11. The maximum current density reached in the alkaline electrolyte is smaller than at pH 3 for the same nitrite concentration, and a peaked signal, positioned at around 0.20 V, replaces the plateau-like measured in acidic media. At pH 13, the current decreases almost to zero when the potential approaches 0 V.

The peak current displays an anomalous dependence on the rotation rate, increasing with *decreasing* ω, without following any clear functional form. For a 50 μM $NaNO_2$ solution, the current increase over the range 2900 – 700 rpm is equal to 46 %. A similar observation has been reported for ammonia oxidation in alkaline media [37]. RRDE experiments comparing the cases E_{disk} = o.c.p. and E_{disk} = 0.20 V show that in the latter case there is an increase both of the peak at E_{ring} = 0.20V and of the oxidative current, (see inset of figure 11). Two oxidation waves can be detected when E_{disk} = 0.20 V, which could be ascribed to the oxidation of two different products, ammonia (at less positive potentials) and HAM. Contrary to the RRDE experiments in acidic media, no shielding effect was noticed.

Finally, OLEMS experiments of nitrite reduction at a stationary Pt electrode showed no signal assignable to N_2O, N_2 and NO.

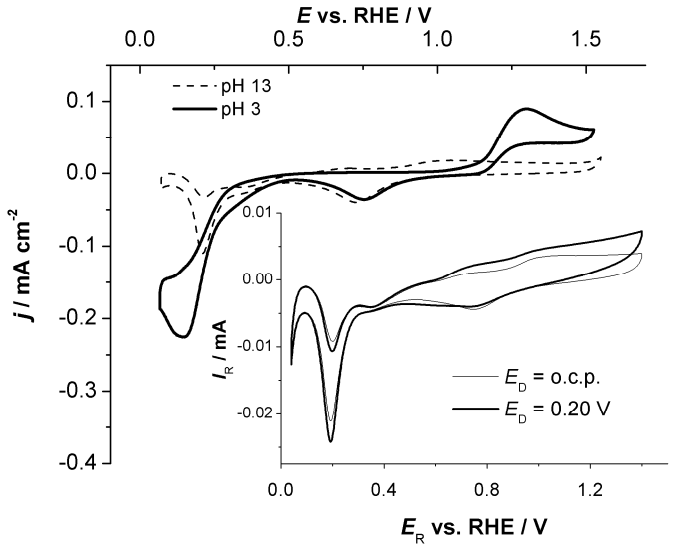

Figure 11 Comparison of voltammetric profiles at a Pt RDE for nitrite reduction in the low-concentration range (50 μM) in a 0.1 M phosphate buffer (pH 3) and in 0.1 M NaOH (pH 13). Inset: comparison of RRDE profiles for nitrite reduction (0.8 mM) in 0.1 M NaOH. Open circuit potential abbreviated as o.c.p. $\omega = 900$ rpm, $v = 10$ mV s^{-1}.

2.4. General discussion of the mechanism

2.4.1 Solution reactions and influence of pH.

Homogeneous-phase reactions need to be taken into account to explain the mechanism of nitrite / nitrous acid reduction in acidic media. These reactions, (Eqs. (1) – (3) in the Introduction), are pH-dependent in a twofold way, both from a thermodynamic and kinetic point of view. A decrease in pH will accumulate nitrous acid, thereby shifting the equilibrium 1 to the right. Therefore, more NO will be formed. Equilibria (2) and (3) play a role at very low pH (<0), as has been argued for the nitrate reduction on Pt in highly acidic media[38].

In addition, the decomposition is acid-catalyzed, possibly via the formation of species such as $H_2NO_2^+$ [14], and the nitrous acid decomposition will be faster in more acidic media. This is clear from Figure 5 and Table 1, where the enhanced

decomposition in acidic media is highlighted both at constant potential (Figure 5) and during cycling experiments, with a more pronounced decomposition at pH 1 than at pH 3.

Hence, under the conditions of the present experiment, the homogeneous-phase reactions, generating a very reactive molecule (NO), must be an integral part of the mechanism, and the kinetics and thermodynamics of NO generation will differ according to the solution pH.

On the other hand, in alkaline media nitrite will be the only "nitrous" solution species, and no other nitrogen-containing molecules will be generated by homogeneous-phase reactions.

2.4.2 The first wave. High-potential formation of N_2O.

FTIRS and OLEMS data reported in this chapter provide clear evidence for the formation of N_2O within the potential region of the first wave (0.3-0.5 V_{RHE}). The reactions leading to this product could involve as many as three species, NO_{ads}, NO_{aq}, and HNO_2.

The formation of an NO adlayer at Pt upon immersion in an acidic nitrite solution is a well-known process[4,21,39]. Transfer experiments performed in this chapter strongly suggest that NO_{ads} plays an important role during nitrite reduction in the acidic pH range. As shown in figure 1, however, the presence of an NO adlayer is a necessary but not a sufficient condition for the first wave to be recorded. Consequently, it is suggested that the process occurring in the high-potential range simultaneously involve adsorbed *and* solution species.

Considering the two solution species available for reactions, HNO_2 (major) and NO_{aq} (minor), two pathways could be proposed to account for N_2O formation, involving NO_{aq} as the main dissolved player:

$$2HNO_{2,aq} \rightarrow NO_{aq} + NO_2 + H_2O \xrightarrow{Pt-surface} NO_{ads} \quad (4a)$$

$$NO_{aq} + NO_{ads} + 2H^+ + 2e^- \rightarrow N_2O + H_2O \quad (4b)$$

or nitrous acid as the solution-phase species reacting with NO_{ads}

$$2HNO_{2,aq} \rightarrow NO_{aq} + NO_2 + H_2O \xrightarrow{Pt-surface} NO_{ads} + NO_2 + H_2O \qquad (4a)$$

$$HNO_{2,aq} + NO_{ads} + 3H^+ + 3e^- \rightarrow N_2O + 2H_2O \qquad (5)$$

where (4b) and (5) are *overall* processes. The reaction (4b) was proposed by De Vooys et al.[21] to explain N_2O formation at Pt in NO-saturated acidic solutions. Obviously, care must be taken in comparing our experimental conditions with those of the study on continuous NO reduction, as in the latter case a saturated NO solution was used. Nevertheless, it is worth noting that, as shown in Figure 4, the first wave does not shift remarkably along the RHE scale, thus displaying a Nernstian dependence also reported for NO continuous reduction.

More insight on the species involved in N_2O formation is obtained by the effect of the pH on the first wave, reported in Figure 4. The major decrease of the first-wave signal taking place at pH 2 does not parallel the dissociation behavior of HNO_2, which is still the dominant species at this pH. Therefore, the pH increase must exert another, more decisive effect in the kinetics. We can argue that NO, both as adsorbate and solution species, is generated more massively at a lower pH, as shown by the much lower NO stripping charge at pH 3. A limited NO coverage and a lower concentration of NO_{aq} due to a more sluggish decomposition would then both contribute to reduce the current of the first-wave signal.

Although no Levich analysis was carried out for the first wave, we can exclude that the first wave is a diffusion-controlled reaction to N_2O. In this case, in fact, a ratio of the diffusion-limited currents of the second and the first wave would be not higher than 3 (6-electron process to NH_4^+ at low potentials and a 2-electron reduction to N_2O). The value obtained here, $j_{\text{second wave}}/j_{\text{first-wave}} = 8.8$ (0.1 M $HClO_4$), exceeds this limit and suggests that a more complex process, limited by a minor solution/surface species (NO), is actually active.

Electrochemical data show that the first wave and the accompanying consumption of nitrous acid are more relevant during the negative-going than the positive-going scan; OLEMS data support that this hysteresis is due to a limited formation of N_2O in the positive-going scan. In addition, the first wave decreases if the electrode potential is swept in the potential region 0.05 – 0.6 V. All this information points to the important role of the timescale of NO formation. This adsorbate is depleted

during the negative-going scan and then only partially recovered during the positive-going scan. This can explain why the slower OLEMS experiment (1 mV s^{-1}) shows a less marked hysteresis than the faster RRDE experiment (10 mV s^{-1}).

The evidence presented and the comparison with related works in the literature support the reaction sequence (4a), (4b) for the generation of N_2O. Thus, NO, and not HNO_2 or NO_2^-, dominates in the electrochemical reactivity in the potential region of the first-wave.

2.4.3 The second reduction wave: Formation of NH_2OH (and NH_3).

The occurrence of hydroxylamine as the main reduction product at low potentials is supported by evidence from our work as well as previous research[1]. Here we will comment on some specific aspects observed in the present work.

The detailed determination of the nature of the process (or the combination of processes) leading to the peaked reduction feature in the negative-going scan was not a topic of concern in this article. Nevertheless, some insight can be deduced by noticing that the peak is invariably followed by a plateau-like current during the earliest stage of the positive-going potential sweep. Therefore, as a peaked feature in a RDE experiment is often explained in terms of adsorbed or poisoning species[37], we propose the following picture:

- Negative-going scan (peak): combined nitrous acid reduction and removal of NO_{ads}.
- Positive going scan (plateau-like): diffusion- or mixed-controlled nitrous acid reduction on the "clean" Pt surface; no NO_{ads} reduction.

Even traces of NO can give adsorbates[40], and this could explain why the peak is seen also in the micro-molar concentration range.

On the basis of the results of the RRDE experiments and the *n* value obtained from Levich plots at low concentration and at pH $\geq$ 3.5, we can confirm, for the reduction plateau-like feature at the lowest potentials, a diffusion-controlled reaction to hydroxylamine, as already reported by Bruckenstein[1], who calculated, for a 0.4 mM nitrite solution in 0.1M $HClO_4$, $n = 3.83$. This $n < 4$ was ascribed to the disproportionation of hydroxylamine. In the present research, *n* decreases

below 4 at pH < 3.5 to a value close to 3; nevertheless, we believe that hydroxylamine is still the main product and the underestimation could be due to:

- An overestimation of the nitrous acid concentration (by its solution phase decomposition).
- Complications in the reaction mechanism owing to the presence of NO_{aq} (reducible at Pt in the same potential range of nitrous acid/nitrite).

The effect of an increase in nitrite concentration is clearly understood by comparing the *y*-axis intercepts of Levich plots: at lower concentrations, the linear plots pass through the origin, as predicted by theory for a purely diffusion-controlled process. At higher concentrations, the linear branch of the Levich plot shows a non-zero intercept: in this case, the current can be thought of as a sum of currents of two processes, one described Levich equation, the other having a current independent of rotation rate[41,42]. The latter is usually a purely chemical step occurring in parallel to the diffusion-controlled process. Within the framework of the present work, it is logical to ascribe the non-zero intercept to the decomposition of nitrous acid to NO. This explanation is however only valid if we assume that it is possible to neglect the acceleration of nitrous acid decomposition due to increased forced convection. Otherwise, the non-linearity of the Levich plot could be also ascribed to this effect of the change in rotation rate.

Interestingly, at higher concentration the process giving rise to the plateau-like current displays a non-trivial pH dependence, with a shift to more negative potentials as the pH increases. Given the high proton demand of nitrous acid reduction (5 protons per molecule when hydroxylamine is the product), nitrous acid reduction is likely to be in competition with hydrogen evolution. The shift to more negative potentials is also expected to bring about a change in selectivity to ammonia, because hydroxylamine converts into this molecule –although slowly – at potentials corresponding to the hydrogen evolution region[34]. Three experimental observations agree with suggesting ammonia as the preferred product when the plateau-like feature is located at a potential more negative than E = 0 V: the number of electrons obtained from a Levich plot at pH 3 (n = 6.0) and the absence of hydroxylamine oxidation current during shielding ring-disk experiments at the same pH. Hence formation of hydroxylamine as the major product is restricted to a

certain pH and *E* range, the potential being influenced in a non-trivial way by the pH.

2.4.4 Alkaline media.

The suppression of the solution-phase reactions drastically changes the reduction characteristics. At pH 13, the only solution species present is the nitrite ion, which seems to be less reactive than the species present in acidic media. The decrease of the peak current with increasing rotation rate could be ascribed to the escape of an intermediate from the electrode surface. This could then account for the increase in peak current at the ring in RRDE experiments when the disk potential is kept at E = 0.20 V. A likely candidate for this intermediate is HAM: ammonia formation was detected during reduction a 10 mM solution of HAM in 0.5 M KOH[43]. HAM can be both oxidized and reduced, thus explaining the results of the RRDE experiments. The absence of a shielding effect, on the other hand, shows that nitrite reduction is not a diffusion-controlled reaction.

The marked decrease in current at potential close to E = 0 V is in agreement with the hypothesis that adsorbed hydrogen acts as a poison for nitrite reduction in alkaline media[44].

2.5. Conclusions.

The electrochemical reduction of nitrous species on Pt can follow different pathways as a function of the electrode potential and the solution pH: in the light of the results of this chapter we suggest a general pH-dependent mechanistic scheme (Scheme 1). In acidic to mildly acidic media, the process is a combination of the intrinsic nitrite / nitrous acid electro-reactivity with a homogeneous phase reaction producing an additional reactive species (NO) from the decomposition of nitrous acid. N_2O is the major product at higher potentials (0.3 - 0.4 V), while NH_2OH dominates at lower potential (0.05-0.10 V). An increase in nitrite concentration, forced convection as well as a decrease in pH enhance the decomposition of nitrous acid. In obtaining these results, combining electrochemical techniques with spectroscopy (FTIRS and online mass spectrometry) was of paramount importance.

In absence of any aqueous-phase reactions, as in alkaline media, the nitrite ion can still be reduced on Pt, although with a lower activity, and the main products are non-volatile species.

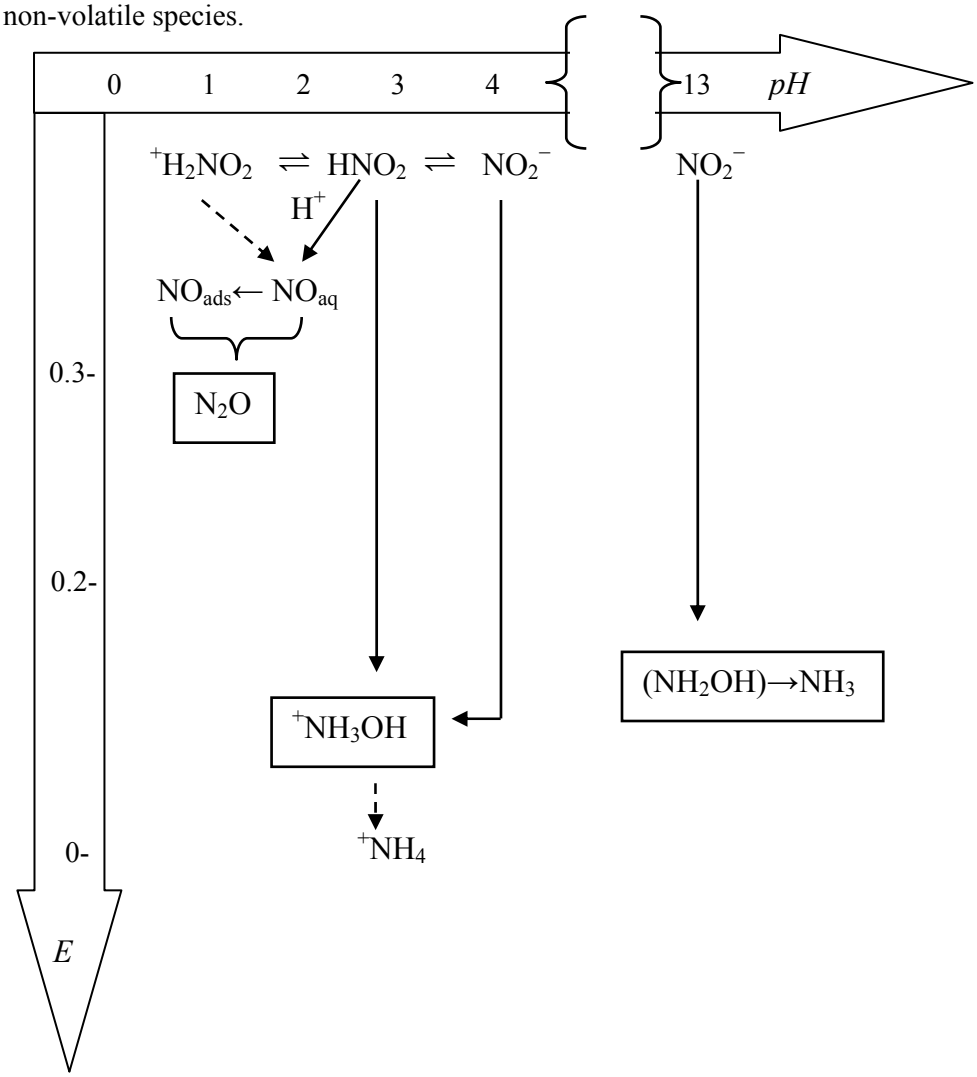

Scheme 1 Mechanistic pathways for nitrite/nitrous acid reduction as a function of pH and potential.

2.6. Acknowledgments

The authors acknowledge partial financial support from the European Commission (through FP7 Initial Training Network "ELCAT", Grant Agreement No. 214936-

2), an Erasmus grant awarded to VK, as well as financial support from the Netherlands Organization for Scientific Research ("NWO-Middelgroot") for the purchase and development of the online electrochemical mass spectrometer.

References

(1) Gadde, R. R.; Bruckenstein, S. *J. Electroanal. Chem.* **1974**, *50*, 163-174.
(2) Kita, H.; Ye, S.; Sugimura, K. *J. Electroanal. Chem.* **1991**, *297*, 283-296.
(3) Petrii, O. A.; Safonova, T. Y. *J. Electroanal. Chem.* **1992**, *331*, 897-912.
(4) Ye, S.; Kita, H. *J. Electroanal. Chem.* **1993**, *346*, 489-495.
(5) da Cunha, M. C. P. M.; Nart, F. C. *Phys. Status Solidi A* **2001**, *187*, 25-32.
(6) Bae, I. T.; Barbour, R. L.; Scherson, D. A. *Anal. Chem.* **1997**, *69*, 249-252.
(7) Rosca, V.; Duca, M.; de Groot, M. T.; Koper, M. T. M. *Chem. Rev.* **2009**, *109*, 2209-2244.
(8) Rodes, A.; Gomez, R.; Orts, J. M.; Feliu, J. M.; Perez, J. M.; Aldaz, A. *Langmuir* **1995**, *11*, 3549-3553.
(9) Dima, G. E.; de Vooys, A. C. A.; Koper, M. T. M. *J. Electroanal. Chem.* **2003**, *554-555*, 15-23.
(10) de Vooys, A. C. A.; van Santen, R. A.; van Veen, J. A. R. *J. Mol. Catal. A: Chem.* **2000**, *154*, 203-215.
(11) Vanderplas, J. F.; Barendrecht, E. *Recl. Trav. Chim. Pays-Bas* **1977**, *96*, 133-136.
(12) Park, J. Y.; Lee, Y. N. *J. Phys. Chem.* **1988**, *92*, 6294-6302.
(13) Beake, B. D.; Moodie, R. B. *J. Chem. Soc., Perkin Trans. 2* **1995**, 1045-1048.
(14) Riordan, E.; Minogue, N.; Healy, D.; O'Driscoll, P.; Sodeau, J. R. *J. Phys. Chem. A* **2005**, *109*, 779-786.
(15) Nishimura, K.; Machida, K.; Enyo, M. *Electrochim. Acta* **1991**, *36*, 877-880.
(16) da Silva, G.; Kennedy, E. M.; Dlugogorski, B. Z. *J. Phys. Chem. A* **2006**, *110*, 11371-11376.
(17) *Handbook of Chemistry and Physics*; 53rd ed. ed.; Weast, R. C., Ed.; The Chemical Rubber, co.: Cleveland, 1972-1973.
(18) Abel, E.; Schmid, H. *Z. Phys. Chem.* **1928**, *134*, 279-300.
(19) Braida, W.; Ong, S. K. *Water, Air, Soil Pollut.* **2000**, *118*, 13-26.
(20) Klemenc, A.; Pollak, F. *Z. Phys. Chem.* **1922**, *101*, 150-171.
(21) de Vooys, A. C. A.; Koper, M. T. M.; van Santen, R. A.; van Veen, J. A. R. *Electrochim. Acta* **2001**, *46*, 923-930.
(22) Lai, S. C. S.; Koper, M. T. M. *Faraday Discuss.* **2009**, *140*, 399-416.
(23) Lebedeva, N. P.; Koper, M. T. M.; Feliu, J. M.; van Santen, R. A. *Electrochem. Commun.* **2000**, *2*, 487-490.
(24) Wonders, A. H.; Housmans, T. H. M.; Rosca, V.; Koper, M. T. M. *J. Appl. Electrochem.* **2006**, *36*, 1215-1221.
(25) Albery, W. J.; Hitcham, M. L. *Ring-Disc Electrodes*; 1st ed. ed.; Oxford University Press: London, 1971.
(26) Piela, B.; Piela, P.; Wrona, P. K. *J. Electrochem. Soc.* **2002**, *149*, E357-E366.
(27) Piela, B.; Wrona, P. K. *J. Electrochem. Soc.* **2002**, *149*, E55-E63.

(28) Bard, A. J.; Faulkner, L. R. *Electrochemical methods : fundamentals and applications*; 2nd ed. ed.; John Wiley & Sons: New York, 2001.
(29) Xing, X. K.; Scherson, D. A. *Anal. Chem.* **1988**, *60*, 1468-1472.
(30) Atkins, P. W. *Physical Chemistry*; 6th ed. ed.; Oxford University Press: Oxford, 1999.
(31) Younathan, J. N.; Wood, K. S.; Meyer, T. J. *Inorg. Chem.* **1992**, *31*, 3280-3285.
(32) Francisco, J. S. *J. Chem. Phys.* **2001**, *115*, 2117-2122.
(33) Nakamoto, K. *Infrared and Raman spectra of inorganic and coordination compounds* 5th ed. ed.; Wiley: New York, 1997.
(34) Rosca, V.; Beltramo, G. L.; Koper, M. T. M. *J. Electroanal. Chem.* **2004**, *566*, 53-62.
(35) Bennett, M. R.; Brown, G. M.; Maya, L.; Posey, F. A. *Inorg. Chem.* **1982**, *21*, 2461-2468.
(36) Raman, S.; Ashcraft, R. W.; Vial, M.; Klasky, M. L. *J. Phys. Chem. A* **2005**, *109*, 8526-8536.
(37) Endo, K.; Katayama, Y.; Miura, T. *Electrochim. Acta* **2005**, *50*, 2181-2185.
(38) de Groot, M. T.; Koper, M. T. M. *J. Electroanal. Chem.* **2004**, *562*, 81-94.
(39) Rodes, A.; Gomez, R.; Perez, J. M.; Feliu, J. M.; Aldaz, A. *Electrochim. Acta* **1996**, *41*, 729-745.
(40) Nakata, K.; Okubo, A.; Shimazu, K.; Yamakata, A.; Ye, S.; Osawa, M. *Langmuir* **2008**, *24*, 4352-4357.
(41) Opekar, F.; Beran, P. *J. Electroanal. Chem.* **1976**, *69*, 1-105.
(42) Medeiros, M. J.; Pletcher, D.; Sidorin, D. *J. Electroanal. Chem.* **2008**, *619*, 83-86.
(43) Wasmus, S.; Vasini, E. J.; Krausa, M.; Mishima, H. T.; Vielstich, W. *Electrochim. Acta* **1994**, *39*, 23-31.
(44) Horanyi, G.; Rizmayer, E. M. *J. Electroanal. Chem.* **1985**, *188*, 265-272.